Supporting Information

Excited State Dynamics of Carotenoids in Light Harvesting Complexes: 1. Exploring the Relationship between the S_1 and S* States

Emmanouil Papagiannakis, Ivo H.M. van Stokkum, Mikas Vengris,
Richard J. Cogdell, Rienk van Grondelle, Delmar S. Larsen

S.1 One-photon models

A long standing difficulty in interpreting complex dynamics measured on ensembles of chromophores (or multi-chromophore complexes like LH2) is whether the observed behavior arises from intrinsic homogeneous or inhomogeneous characteristics of the sample. In general, it is difficult to separate these contributions without the aid of additional studies like non-linear,[1-3] hole burning[4] or single-molecule[5] experiments. The simple three-state homogenous model ($S_2 \rightarrow S_1 \rightarrow S_0$,) used to describe electronic excited state relaxation in carotenoids until recently, fails to capture many of the spectroscopic observations of the last few years. Recently, additional states and complex branched dynamical schemes have been introduced in the description[6,7] however, further complications arising from ground-state inhomogeneous populations have thus far been avoided; here we show how these can be addressed with excitation-intensity dependent PP measurements.

To interpret the excitation intensity dependence of the 4-ps transient absorption spectrum in Figure 4, we consider two simplified one-photon models: homogeneous and inhomogeneous (Fig. S1). The homogeneous model (Fig. S1A) is the most direct and common approach in interpreting the complex excited state dynamics of carotenoids in LH complexes,[8-11] whereby the S_2 excited state population simultaneously decays (*i.e.* in parallel) into two or more lower lying electronic states (S* and S_1). This simple model entails establishing a branching ratio to determine population flow from the S_2 state and then explaining the observed dynamics as a result from exciting a single ground-state population. A set of differential equations to describe the population flow in this branched, homogenous, simplified model can easily be constructed:

$$\frac{d[S_2]}{dt} = \mu I(t)\{[S_0]-[S_2]\} - \boldsymbol{k}_{2\rightarrow 1}[S_2] - \boldsymbol{k}_{2\rightarrow S^*}[S_2] \qquad \text{(S1a)}$$

$$\frac{d[S_1]}{dt} = \boldsymbol{k}_{2\rightarrow 1}[S_2] - \boldsymbol{k}_{1\rightarrow 0}[S_1] \qquad \text{(S1b)}$$

$$\frac{d[S^*]}{dt} = \boldsymbol{k}_{2\to S^*}[S_2] - \boldsymbol{k}_{S^*\to 0}[S^*] \qquad \text{(S1c)}$$

$$\frac{d[S_0]}{dt} = -\mu I(t)\{[S_0]-[S_2]\} + \boldsymbol{k}_{1\to 0}[S_1] + \boldsymbol{k}_{S^*\to 0}[S^*] \qquad \text{(S1d)}$$

where $[S_i]$ (i= 0, 1, 2) denote the population of the S_0, S_1 and S_2 electronic states respectively, and [S*] the population of the S* state. S_0 and S_2 are coupled via the external electric field of the laser pulse (with an extinction coefficient, μ) with a Gaussian time-dependent profile, $I(t)$. The decay time constants: $k_{2\to 1}$, $k_{2\to S^*}$, $k_{1\to 0}$ and $k_{S^*\to 0}$ represent the decay timescales from S_2 to S_1, S_2 to S*, S_1 to S_0, and S* to S_0 respectively.

In contrast, the inhomogeneous model postulates that the observed dynamics results from the simultaneous excitation of two ground-state sub-populations (S_0, S_0*), each evolving with different dynamics (Fig. 1B). The corresponding differential equations that describe the population flow in such an inhomogeneous model are more complex than in the previous homogeneous model:

$$\frac{d[S_2]}{dt} = \mu I(t)\{[S_0]-[S_2]\} - \boldsymbol{k}_{2\to 1}[S_2] \qquad \text{(S2a)}$$

$$\frac{d[S_2^*]}{dt} = \mu^* I(t)\{[S_0^*]-[S_2^*]\} - \boldsymbol{k}_{2\to S^*}[S_2^*] \qquad \text{(S2b)}$$

$$\frac{d[S_1]}{dt} = \boldsymbol{k}_{2\to 1}[S_2] - \boldsymbol{k}_{1\to 0}[S_1] \qquad \text{(S2c)}$$

$$\frac{d[S^*]}{dt} = \boldsymbol{k}_{2\to S^*}[S_2^*] - \boldsymbol{k}_{S^*\to 0^*}[S^*] \qquad \text{(S2d)}$$

$$\frac{d[S_0]}{dt} = -\mu I(t)\{[S_0]-[S_2]\} + \boldsymbol{k}_{1\to 0}[S_1] \qquad \text{(S2e)}$$

$$\frac{d[S_0^*]}{dt} = -\mu^* I(t)\{[S_0^*]-[S_2^*]\} + \boldsymbol{k}_{S^*\to 0^*}[S^*] \qquad \text{(S2f)}$$

(with extinction coefficients μ and μ*) and two S_0 and S_2 states. Neither simplified model includes the intermediate states populated after EET such as the excited states of the B800 or the Q_x of the B850 bacteriochlorophylls, nor additional contributions from B850 exciton and

annihilation dynamics[12] or other carotenoid transient states (*e.g.* $1B_u^-$, $3A_g^-$, hot S_1, triplets).[9,13] Although highly simplified, these two models illustrate how the homogeneous and inhomogeneous schemes can be determined with intensity-dependent PP measurements; more complete models for the LH2 dynamics that incorporate the full time-resolved PP data are discussed in main text.

The population dynamics predicted by the homogenous model (symbols) and the dynamics predicted by the inhomogeneous model (lines) using three different sets of parameters (Table SI) are compared in Figure S1C. Although the underlying models and parameters differ for the four cases considered, the predicted population dynamics are essentially indistinguishable (symbols *vs.* lines). It is clear that the nature of the underlying dynamics cannot be unequivocally determined by solely fitting the different models to the PP population kinetics. It should be noted that the inhomogeneous model requires the inclusion of additional states (two ground-states: S_0 and S_0*, and two excited-states: S_2 and S_2*) into the model as opposed to the homogeneous model. This added complexity in modeling was sufficient to exclude the feasibility of implementing the inhomogeneous model in many previous studies of carotenoids dynamics.

Although the population dynamics alone are not enough to differentiate these models, we show that by exploring the relative excitation-intensity dependent characteristics of the simulated signals, the different models *may* be distinguished. In the homogeneous model, the observed dynamics is initiated by the excitation of a single ground-state population, hence the predicted power dependence of the S* and S_1 signals follows identical saturation curves (Fig. S1D, overlapping solid lines). For the inhomogeneous model with the same extinction coefficients for each sub-population, the predicted power dependence is identical with the homogeneous model (Fig. S1D, overlapping symbols). However, if the observed dynamics results from the excitation of multiple ground-state populations with *different* extinction coefficients, then by increasing the excitation intensity, one sub-population saturates at a lower intensity than the other (Fig. S1E-F). Thus, by comparing the different saturation behavior of the band in the self-referenced dispersed PP data in Figure 3, we may attribute the observed complex dynamics to inhomogeneity and estimate the relative extinction coefficients and relative occupation of the each sub-population. All assuming the inhomogeneous model is applicable for describing the underlying dynamics of the LH2 system.

S2. Global analysis

An important goal of studying multi-chromophore systems is to identify and characterize the connectivity between the constituent states. In order to elucidate such details about the system under investigation, we used a sophisticated multi-wavelength global analysis approach to fit a postulated dynamical model with discrete transient states to the collected pump-probe data.[14-16] Central to this type of analysis is the construction of a connectivity scheme, k_{ij} that describes the interactions between the observed time-resolved states, $n_j(t)$. Assuming first order rate kinetics, a series of differential equations which describe the time evolution of the constituent transient states is constructed and numerically solved (MATLAB):

$$\dot{n}_i(t) = \sum_j k_{ij} n_j(t). \qquad \text{(S3)}$$

Spectral information is then introduced by adding explicit wavelength dependence to the obtained solution, resulting in the generation of wavelength-dependent factors to the time-dependent population dynamics.

$$D(\lambda, t; k_{ij}) = \sum_i A_i(\lambda) n_i(t; k_{ij}) \qquad \text{(S4)}$$

where $D(\lambda, t; k_{ij})$ is the absorption difference signal that can directly be compared with the experimentally collected data. The resulting wavelength-dependent factor, $A_i(\lambda)$, is the Species Associated Difference Spectrum (SADS) for the i^{th} transient state. The SADS in combination with the connectivity scheme and the corresponding decay times provide an easy approach for interpreting the complex dispersed pump-probe data collected in our experiment. The SADS and timescales that relate the growth and decay kinetics associated with these individual states are estimated from the data by means of nonlinear regression. An important underlying aspect of this approach is that the measured signals can be decomposed into a set of connected states/species with corresponding decay times and spectra.

S2.1: Differential equations

The corresponding differential equations for the homogeneous model (Fig. 5A) used to describe the LH2 dynamics that were used to globally analyze the PP kinetics of LH2 are described in Eq. S5.

$$\frac{d[S_2]}{dt} = I(t)\mu\left([S_0]-[S_2]\right) - \boldsymbol{k}_{S_2\to S^*}[S_2] - \boldsymbol{k}_{S_2\to S_{Hot}}[S_2] - \boldsymbol{k}_{S_2\to B850}[S_2] \quad \text{(S5a)}$$

$$\frac{d[S_{Hot}]}{dt} = \boldsymbol{k}_{S_2\to S_{Hot}}[S_2] - \boldsymbol{k}_{S_{Hot}\to S_1}[S_{Hot}] - \boldsymbol{k}_{S_{Hot}\to B850}[S_{Hot}] \quad \text{(S5b)}$$

$$\frac{d[S_1]}{dt} = \boldsymbol{k}_{S_{Hot}\to S_1}[S_{Hot}] - \boldsymbol{k}_{S_1\to S_0}[S_1] - \boldsymbol{k}_{S_1\to B850}[S_1] \quad \text{(S5c)}$$

$$\frac{d[S^*]}{dt} = \boldsymbol{k}_{S_2\to S^*}[S_2] - \boldsymbol{k}_{S^*\to S_0}[S^*] - \boldsymbol{k}_{S^*\to T}[S^*] - \boldsymbol{k}_{S^*\to B850}[S^*] \quad \text{(S5d)}$$

$$\frac{d[T]}{dt} = \boldsymbol{k}_{S^*\to T}[S^*] \quad \text{(S5e)}$$

$$\begin{aligned}\frac{d[S_0]}{dt} = &-I(t)\mu\left([S_0]-[S_2]\right) + \boldsymbol{k}_{S_1\to S_0}[S_1] + \boldsymbol{k}_{S^*\to S_0}[S^*] \\ &+ \boldsymbol{k}_{S_2\to B850}[S_2] + \boldsymbol{k}_{S_{Hot}\to B850}[S_{Hot}] + \boldsymbol{k}_{S_1\to B850}[S_1] + \boldsymbol{k}_{S^*\to B850}[S^*]\end{aligned} \quad \text{(S5f)}$$

$$\frac{d[B850]}{dt} = \boldsymbol{k}_{S_2\to B850}[S_2] + \boldsymbol{k}_{S_{Hot}\to B850}[S_{Hot}] + \boldsymbol{k}_{S_1\to B850}[S_1] + \boldsymbol{k}_{S^*\to B850}[S^*] \quad \text{(S5g)}$$

where S_i (i=0,1,2) is the population of the S_0, S_1 and S_2 electronic states, respectively and B850 is the population of the final energy acceptor state. The S_0 and S_2 electronic states are coupled via the external electric field of the laser pulses (with a normalized extinction coefficient). The excitation profile, $I(t)$, is assumed Gaussian. The parameters used in this model are tabulated in Table 2 in the main text. The fits of the homogenous and inhomogeneous models in Fig. 5A,B, overlapping with the measured time-resolved PP data, are shown in Figure SI2.

The differential equations used in the inhomogeneous model (Fig. 5B) differ slightly:

$$\frac{d[S_2]}{dt} = I(t)\mu\left([S_0]-[S_2]\right) - \boldsymbol{k}_{S_2\to S_{Hot}}[S_2] - \boldsymbol{k}_{S_2\to B850}[S_2] \quad \text{(S6a)}$$

$$\frac{d[S_2^*]}{dt} = I(t)\mu^*\left\{[S_0^*]-[S_2^*]\right\} - \boldsymbol{k}_{S_2^*\to S^*}[S_2^*] - \boldsymbol{k}_{S_2^*\to B850}[S_2^*] \quad \text{(S6b)}$$

$$\frac{d[S_{Hot}]}{dt} = \boldsymbol{k}_{S_2\to S_{Hot}}[S_2] - \boldsymbol{k}_{S_{Hot}\to S_1}[S_{Hot}] - \boldsymbol{k}_{S_{Hot}\to B850}[S_{Hot}] \quad \text{(S6c)}$$

$$\frac{d[S_1]}{dt} = \boldsymbol{k}_{S_{Hot}\to S_1}[S_{Hot}] - \boldsymbol{k}_{S_1\to S_0}[S_1] - \boldsymbol{k}_{S_1\to B850}[S_1] \quad \text{(S6d)}$$

$$\frac{d[S^*]}{dt} = \boldsymbol{k}_{S_2^*\to S^*}[S_2] - \boldsymbol{k}_{S^*\to S_0^*}[S^*] - \boldsymbol{k}_{S^*\to T}[S^*] - \boldsymbol{k}_{S^*\to B850}[S^*] \quad \text{(S6e)}$$

$$\frac{d[T]}{dt} = \boldsymbol{k}_{S^*\to T}[S^*] \quad \text{(S6f)}$$

$$\begin{aligned}\frac{d[S_0]}{dt} = &-I(t)\mu\left([S_0]-[S_2]\right) + \boldsymbol{k}_{S_1\to S_0}[S_1] + \boldsymbol{k}_{S^*\to S_0}[S^*] \\ &+ \boldsymbol{k}_{S_2\to B850}[S_2] + \boldsymbol{k}_{S_{Hot}\to B850}[S_{Hot}] + \boldsymbol{k}_{S_1\to B850}[S_1] + \boldsymbol{k}_{S^*\to B850}[S^*]\end{aligned} \quad \text{(S6g)}$$

$$\frac{d[S_0^*]}{dt} = -I(t)\mu^*\left([S_0]-[S_2]\right) + \boldsymbol{k}_{S^*\to S_0^*}[S^*] + \boldsymbol{k}_{S_2^*\to B850}[S_2^*] + \boldsymbol{k}_{S^*\to B850}[S^*] \quad \text{(S6h)}$$

$$\frac{d[B850]}{dt} = \boldsymbol{k}_{S_2\to B850}[S_2] + \boldsymbol{k}_{S_{Hot}\to B850}[S_{Hot}] + \boldsymbol{k}_{S_1\to B850}[S_1] + \boldsymbol{k}_{S^*\to B850}[S^*] \quad \text{(S6i)}$$

For completeness, the differential equations underlying the two-photon model are

$$\frac{d[S_2]}{dt} = \mu I(t)\left\{[S_0]-[S_2]\right\} - \mu^{ESA} I(t)\left\{[S_2]-[S_n]\right\} - \boldsymbol{k}_{2\to 1}[S_2] - \boldsymbol{k}_{2\to S^*}[S_2] \quad \text{(S7a)}$$

$$\frac{d[S_1]}{dt} = \boldsymbol{k}_{2\to 1}[S_2] + \boldsymbol{k}_{n\to 1}[S_n] - \boldsymbol{k}_{1\to 0}[S_1] \quad \text{(S7b)}$$

$$\frac{d[S^*]}{dt} = \boldsymbol{k}_{2\to S^*}[S_2] + \boldsymbol{k}_{n\to S^*}[S_n] - \boldsymbol{k}_{S^*\to 0}[S^*] \quad \text{(S7c)}$$

$$\frac{d[S_0]}{dt} = -\mu I(t)\{[S_0] - [S_2]\} + \boldsymbol{k}_{1\to 0}[S_1] + \boldsymbol{k}_{S^*\to 0}[S^*] \quad \text{(S7d)}$$

$$\frac{d[S_n]}{dt} = \mu^{ESA} I(t)\{[S_s] - [S_n]\} + \boldsymbol{k}_{n\to S^*}[S_n] + \boldsymbol{k}_{n\to 1}[S_n] \quad \text{(S7e)}$$

$$\frac{d[T]}{dt} = \boldsymbol{k}_{S^*\to T}[S^*] \quad \text{(S6f)}$$

$$\frac{d[B850]}{dt} = \boldsymbol{k}_{S_2\to B850}[S_2] + \boldsymbol{k}_{S_{Hot}\to B850}[S_{Hot}] + \boldsymbol{k}_{S_1\to B850}[S_1] + \boldsymbol{k}_{S^*\to B850}[S^*] \quad \text{(S7g)}$$

Annihilation dynamics occurring due to inter-chlorophyll interactions in the B850 ring are excluded within these models and are introduced in Paper II.

S3. Other carotenoid-containing systems

Other light harvesting proteins from purple bacteria exhibit a saturation behavior similar to LH2 in *Rs. acidophila* with respect to the generation of S_1 and S*. In the LH1 complex of *Rs. Rubrum* and the LH2 complex of *Rb. sphaeroides,* two other LH proteins that exhibit S*,[8,9] the S_1 signals saturate at lower intensities than the corresponding S* signals. The normalized intensity dependent transient absorption spectra of these proteins (Figure S3) highlight this trend, which is remarkably similar to normalized spectra measured for LH2 samples isolated from *Rbs. acidophila* in Figure 4. Clearly, the behavior of these LH systems is similar to that of the *Rps. acidophila* LH2.

The intensity dependences of two other "new" states in different carotenoids were also explored. In strong contrast to the S* state observed in the studied LH proteins, the $S^‡$ observed in β-carotene in hexane[17] and the ICT state observed in peridinin in methanol[18,19] both exhibit purely homogeneous responses (Figure S4). All excitation intensities used for exciting peridinin give identical (normalized) PP spectra. However, the β-carotene transient absorption spectrum does exhibit a weak intensity dependence; even though both the S_1 (at 551 nm) and the $S^‡$ (at 505 nm) ESAs are generated with an intensity-independent yield, the GSB does increase at elevated excitation intensities compared to the other bands. We ascribe

this trend to a weak resonantly enhanced two-photon transition, just like in the two-photon model but resulting in ionization, not just a different branching yield.[20] In this case, two 400-nm excitation photons are absorbed (one that promotes $S_0 \rightarrow S_2$ and the other promoting $S_2 \rightarrow S_n$), which results in the ionization of the carotenoids (12,000 cm^{-1} more energy than two 525-nm photons). A similar multi-photon ionization that results in enhanced bleach signals has previously been observed in visible pump-repump probe experiments of carotenoids in solution.[17] The homogeneous nature of these additional states contrasts with the S* state and lends credence to the earlier claims that the corresponding new electronic states in these systems are formed directly from the respective initially excited S_2 state.[17,23]

Table S1: Simple Model Parameters

Model	$k_{2\rightarrow 1}$	$k_{2\rightarrow S}$*	$k_{1\rightarrow 0}$	$k_{S}*_{\rightarrow 0}$	μ=1	μ*=1	(S_0/S_0*)
Homogeneous	60 fs	60 fs	3 ps	30 ps	1	-	-
Inhomo: #1	30 fs	30 fs	3 ps	30 ps	1	1	50/50
Inhomo: #2	30 fs	30 fs	3 ps	30 ps	0.77	1.43	40/60
Inhomo: #3	30 fs	30 fs	3 ps	30 ps	1.43	0.77	60/40

Simulation parameters used for Figure 6 with the models depicted in Figure 5. Parameters were selected to mirror the dynamics for LH2 isolated from *Rps. acidophila.*

Figure Captions

Figure S1.

The model one-photon connectivity schemes used to interpret the observed intensity dependent data. A) A homogeneous 4-state model with a single S_0 ground state and a single S_2 excited state. B) an inhomogeneous 6-state model that incorporates two distinct ground-state (S_0) populations and two S_2 excited states. C) Simulated kinetics of the homogeneous (symbols) and inhomogeneous model (solid lines) with the three different parameter sets described in Table S1. The pulse duration was set to 30 fs and the pulse peak intensity was 15 a.u. All four simulations generate near identical kinetics curves. For the inhomogeneous models, the S_0 and S_2 states were combined for comparison with the homogenous model. D-F) Simulated intensity dependence of the models. The solid lines are the curves corresponding to the homogeneous model and the symbols represent the different realizations of the inhomogeneous model. The curves were scaled to the same initial slope which represents the "linear" regime for the signals.

Figure S2.

Comparison of fit and PP data of LH2 at select wavelengths. Experimental 525-nm pumped data (solid lines) overlaps the global analysis fit (dashed lines) from all three proposed models. Note that the time scale is linear from -0.5 ps to 0.5 ps, and then logarithmic to 500 ps.

Figure S3.

Normalized excitation intensity-dependent transient absorption spectra for A) LH2 complexes of *Rb. sphaeroides* excited at 505 nm and probed at 5 ps, and B) LH1-RC membrane fragments of *Rs. rubrum* excited at 530 nm and probed at 2 ps. The arrows indicate trends with decreasing pulse intensities.

Figure S4.

Normalized excitation intensity dependent transient absorption spectra for A) β-carotene in hexane at 5 ps and B) peridinin in methanol at 3 ps, both excited at 400 nm. The arrow indicates the trend with increasing pulse intensity.

References

(1) Cho, M.; Scherer, N. F.; Fleming, G. R.; Mukamel, S. *Journal of Chemical Physics* **1992**, *96*, 5618.

(2) Tanimura, Y.; Mukamel, S. *Journal of Chemical Physics* **1993**, *99*, 9496.

(3) Mukamel, S. *Principles of nonlinear optical spectroscopy*; Oxford University Press: New York, 1995.

(4) Jankowiak, R.; Hayes, J. M.; Small, G. J. *Chemical Reviews* **1993**, *93*, 1471.

(5) Barbara, P. F.; Hu, D. H.; Yu, J.; Song, N. W. *Abstracts of Papers of the American Chemical Society* **2001**, *221*, U261.

(6) Polívka, T.; Sundström, V. *Chemical Reviews* **2004**, *104*, 2021.

(7) Hashimoto, H.; Yanagi, K.; Yoshizawa, M.; Polli, D.; Cerullo, G.; Lanzani, G.; De Silvestri, S.; Gardiner, A. T.; Cogdell, R. J. *Archives of Biochemistry and Biophysics* **2004**, *430*, 61.

(8) Gradinaru, C. C.; Kennis, J. T. M.; Papagiannakis, E.; van Stokkum, I. H. M.; Cogdell, R. J.; Fleming, G. R.; Niederman, R. A.; van Grondelle, R. *Proceedings of the National Academy of Sciences of the United States of America* **2001**, *98*, 2364.

(9) Papagiannakis, E.; Kennis, J. T. M.; van Stokkum, I. H. M.; Cogdell, R. J.; van Grondelle, R. *Proceedings of the National Academy of Sciences of the United States of America* **2002**, *99*, 6017.

(10) Wohlleben, W.; Buckup, T.; Herek, J. L.; Cogdell, R. J.; Motzkus, M. *Biophysical Journal* **2003**, *85*, 442.

(11) Rondonuwu, F. S.; Yokoyama, K.; Fujii, R.; Koyama, Y.; Cogdell, R., J,; Watanabe, Y. *Chemical Physics Letters* **2004**, *390*, 314.

(12) van Amerongen, H.; Valkunas, L.; van Grondelle, R. *Photosynthetic Excitons*; World Scientific: Singapore, 2000.

(13) Koyama, Y.; Rondonuwu, F. S.; Fujii, R.; Watanabe, Y. *Biopolymers* **2004**, *74*, 2.

(14) van Stokkum, I. H. M.; Larsen, D. S.; van Grondelle, R. *Biochim Biophys Acta* **2004**, *1657*, 82.

(15) Holzwarth, A. R. Data Analysis in time-resolved measurements. In *Biophysical Techniques in Photosynthesis*; Amesz, J., Hoff, A. J., Eds.; Kluwer: Dordrecht, The Netherlands, 1996.

(16) Hoff, W. D.; van Stokkum, I. H. M.; van Ramesdonk, H. J.; van Brederode, M. E.; Brouwer, A. M.; Fitch, J. C.; Meyer, T. E.; van Grondelle, R.; Hellingwerf, K. J. *Biophys J* **1994**, *67*, 1691.

(17) Larsen, D. S.; Papagiannakis, E.; van Stokkum, I. H. M.; Vengris, M.; Kennis, J. T. M.; van Grondelle, R. *Chemical Physics Letters* **2003**, *381*, 733.

(18) Bautista, J. A.; Hiller, R. G.; Sharples, F. P.; Gosztola, D.; Wasielewski, M.; Frank, H. A. *Journal of Physical Chemistry A* **1999**, *103*, 2267.

(19) Zigmantas, D.; Polívka, T.; Hiller, R. G.; Yartsev, A.; Sundström, V. *Journal of Physical Chemistry A* **2001**, *105*, 10296.

(20) Larsen, D. S.; Vengris, M.; van Stokkum, I. H. M.; van der Horst, M.; Cordfunke, R.; Hellingwerf, K. J.; van Grondelle, R. *Chemical Physics Letters* **2003**, *369*, 563.

(21) Wohlleben, W.; Buckup, T.; Hashimoto, H.; Cogdell, R. J.; Herek, J. L.; Motzkus, M. *Journal of Physical Chemistry B* **2004**, *108*, 3320.

(22) Wohlleben, W.; Buckup, T.; Herek, J. L.; Motzkus, M. *Chemphyschem* **2005**, *6*, 850.

(23) Papagiannakis, E.; Larsen, D. S.; van Stokkum, I. H. M.; Vengris, M.; Hiller, R. G.; van Grondelle, R. *Biochemistry* **2004**, *43*, 15303.

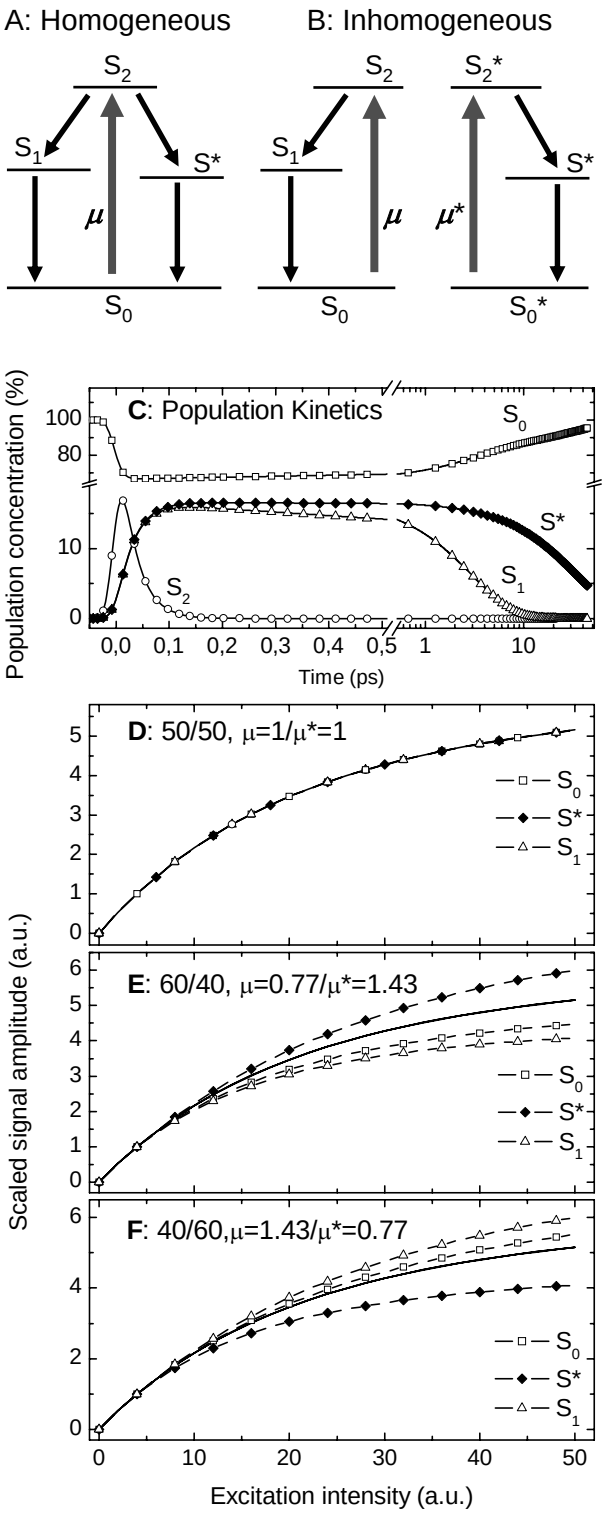

Papagiannakis et al. Fig. S1

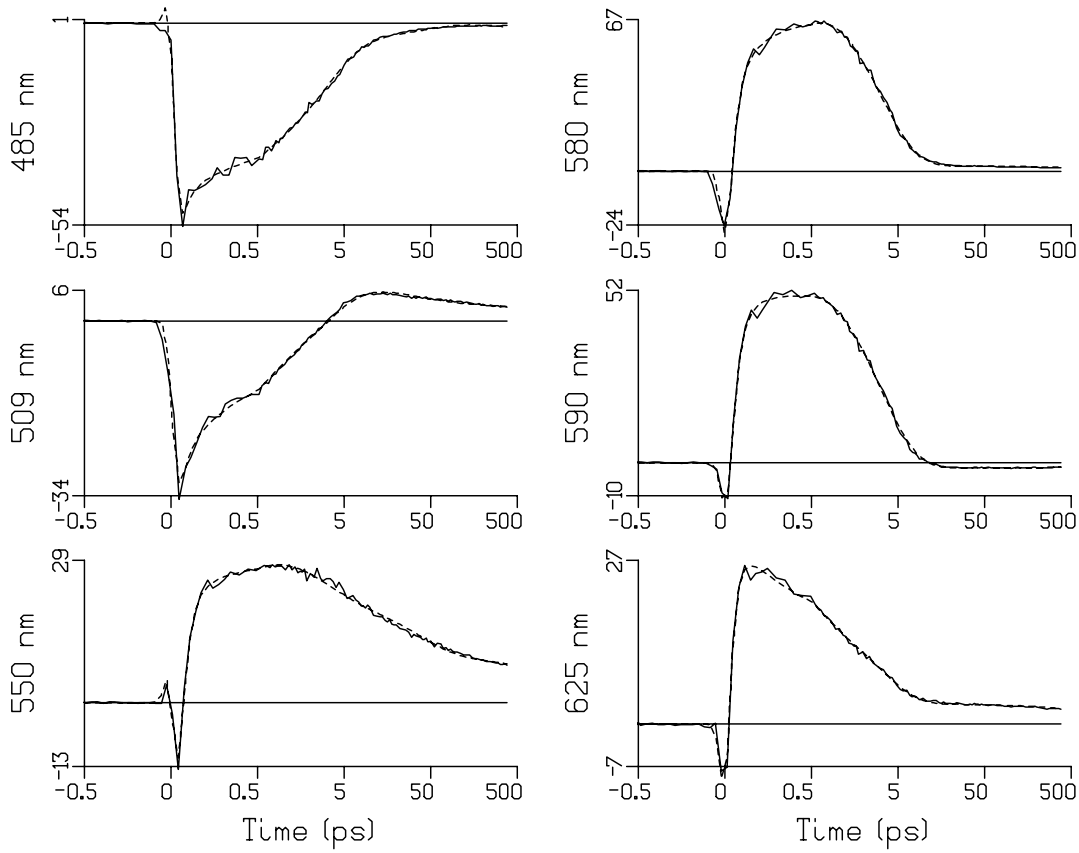

Papagiannakis et al, Fig S2

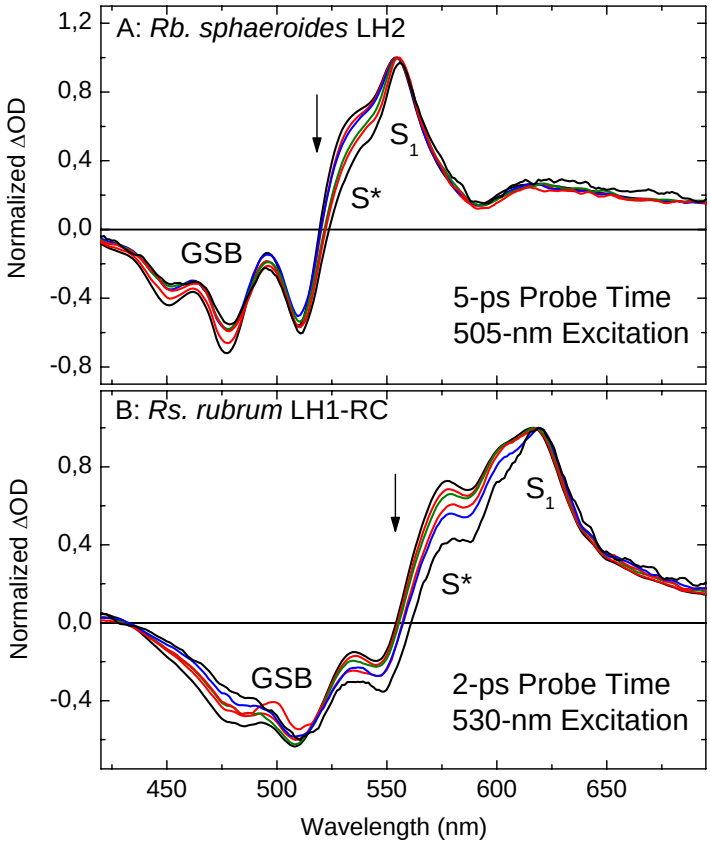

Papagiannakis et al. Fig. S3

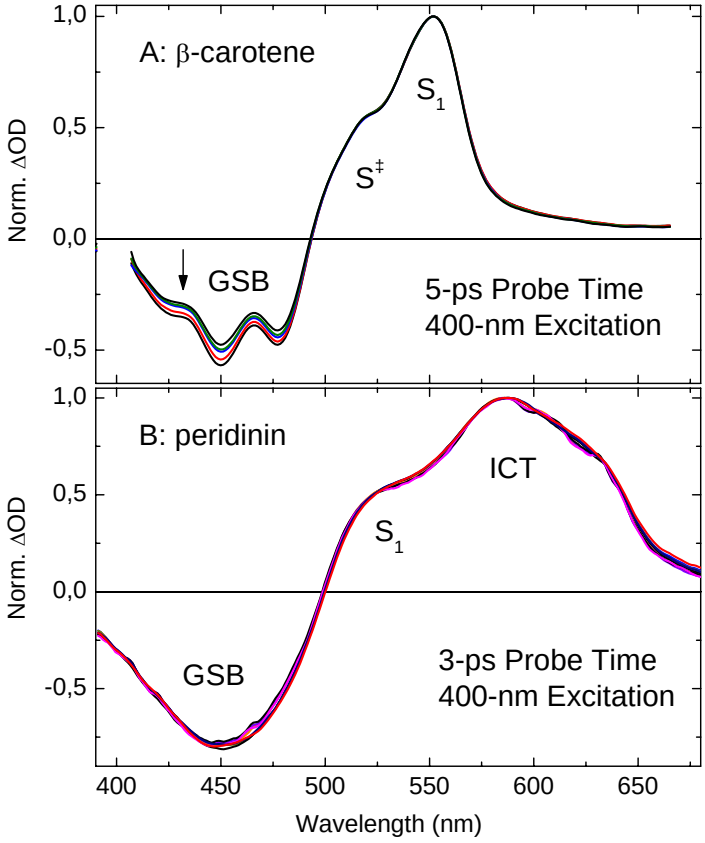

Papagiannakis et al, Fig S4